ChemComm

Accepted Manuscript

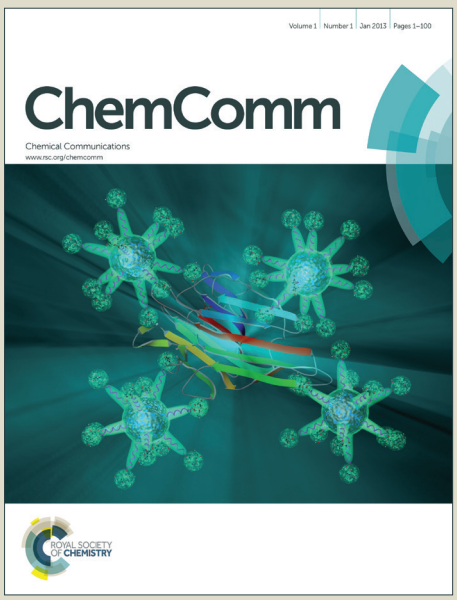

ROYAL SOCIETY OF CHEMISTRY

www.rsc.org/chemcomm

ChemCommun

RSCPublishing

COMMUNICATION

"Suspended" Pt nanoparticles over TiO_2 nanotubes for enhanced photocatalytic H_2 evolution

Cite this: DOI: 10.1039/xoxxoooooox

Nhat Truong Nguyen,[a] JeongEun Yoo,[a] Marco Altomare[a] and Patrik Schmuki*[ab]

Received ooth January 2012,
Accepted ooth January 2012

DOI: 10.1039/xoxxoooooox

www.rsc.org/

In the present work we introduce a technique to form a photocatalyst based on Pt nanoparticles suspended over the mouth of anodic TiO_2 nanotubes. These structures are obtained by decorating the top-end of highly ordered TiO_2 nanotubes with a web of TiO_2 nanofibrils, followed by sputter deposition of a minimum amount of Pt. A subsequent thermal dewetting step forms 3–6 nm-sized Pt nanoparticles along the nanofibrils. These structures, when compared to conventional Pt decoration techniques of TiO_2 nanotubes, show strongly enhanced photocatalytic H_2 evolution efficiency.

Ever since the ground-breaking report by Fujishima and Honda in 1972, TiO_2 has been increasingly investigated for the conversion of solar light into electrical and chemical energy (*e.g.*, photocatalysis, photo-electrochemistry).[1-3] A key advantage of TiO_2 over other semiconductive systems is that except for the proper matching of band-edge positions with respect to H_2O red-ox potentials, it has a very high chemical stability that almost completely suppresses photocorrosion. In aqueous environments, under UV or solar light irradiation, electrons and holes generated in TiO_2 conduction and valence bands, respectively, are able to split water into H_2 and O_2.[4-6] Usually TiO_2 photocatalysts are mainly based on powders. However, one-dimensional morphologies, such as nanowires, nanorods and nanofibers were recently shown to exhibit preferential percolation pathways for charge carrier separation, hence resulting in highly photoactive materials.[7]

One of the most investigated structures over the past few years are ordered TiO_2 nanotube arrays formed by anodization of Ti substrates in adequate electrolytes. Early works of Assefpour-Dezfuly *et al.* and Zwilling *et al.* already provided the basis for the growth of TiO_2 nanotubes by anodizing Ti in dilute fluoride-containing electrolytes.[8,9] Afterwards, growth conditions have been widely investigated in order to fabricate TiO_2 nanotubes with a large range of different structural and morphological features.[3] Anodic TiO_2 nanostructures not only have shown favorable electron transport but also have been reported to show a better photocatalytic activity compared to TiO_2 nanoparticle layers.[10-12]

Nevertheless, if any TiO_2 structures are used towards photocatalysis for water splitting, the deposition of a co-catalyst is required to achieve a reasonable H_2 efficiency. In particular, the deposition of Pt nanoparticles on TiO_2 leads to drastically more effective H_2 production. This is typically ascribed to following two reasons: *i)* Pt nanoparticles are able to trap conduction band electrons and to mediate their transfer to the liquid phase; *ii)* Pt sites represent efficient catalytic sites for the recombination of atomic hydrogen to H_2.[4,13-17] TiO_2 structures are thus decorated with Pt using photo-deposition, electro-deposition, sol-gel techniques and impregnation.[18-20]

In the present work, we introduce a novel Pt@TiO_2 nanotube platform that provides higher H_2 evolution efficiencies than conventional approaches. Our goal was an efficient decoration of TiO_2 with a minimum amount of Pt. For this we present an approach that leads to nanoparticles suspended over the top opening of TiO_2 nanotubes as shown in Fig. 1. To fabricate this structure we used a processing sequence as outlined in scheme 1. Tubes, grown by electrochemical anodization, were firstly subjected to a simple chemical treatment in alkaline solution which allowed for the formation of a TiO_2 nanofibril web at the mouth of the tubes. Then, sputter-deposition was employed to decorate the nanofibrils with minimal amounts of Pt. The Pt decoration then was converted into 3-6 nm-sized Pt nanoparticles by a thermal dewetting step. The photocatalytic H_2 evolution efficiency from these structures was then compared to conventional Pt decoration techniques of TiO_2 nanotubes.

Fig. 1 shows SEM and TEM images of the nanostructures at each stage of their fabrication. Highly ordered TiO_2 nanotubes (see Fig. S1) were produced by anodization of Ti in hot HF/H_3PO_4 mixtures (Fig. 1(a) and (b)). These nanotubes have a diameter of ~ 80 nm and a height of ~ 200 nm, and show a reaction-vessel geometry that was demonstrated to be optimal for UV light-driven photocatalysis.[21,22]

If these tube layers (after a first mild annealing in air) are exposed to a strongly alkaline solution (4 M $NaOH_{aq}$), TiO_2 nanofibrils form across the openings of the tubes (Fig. 1(c)).[23,24] In our case, this results in a web-like structure that consists of *ca*. 5 nm-wide fibrils (Fig. 1(h)). It should be pointed out that the air-annealing step is of crucial importance. As-formed, *i.e.*, amorphous, nanotubes were strongly damaged after a 30 min-NaOH soaking (with only a negligible nanofibril formation) and totally destroyed after 24 h (Fig. S2 (c)-(e)).

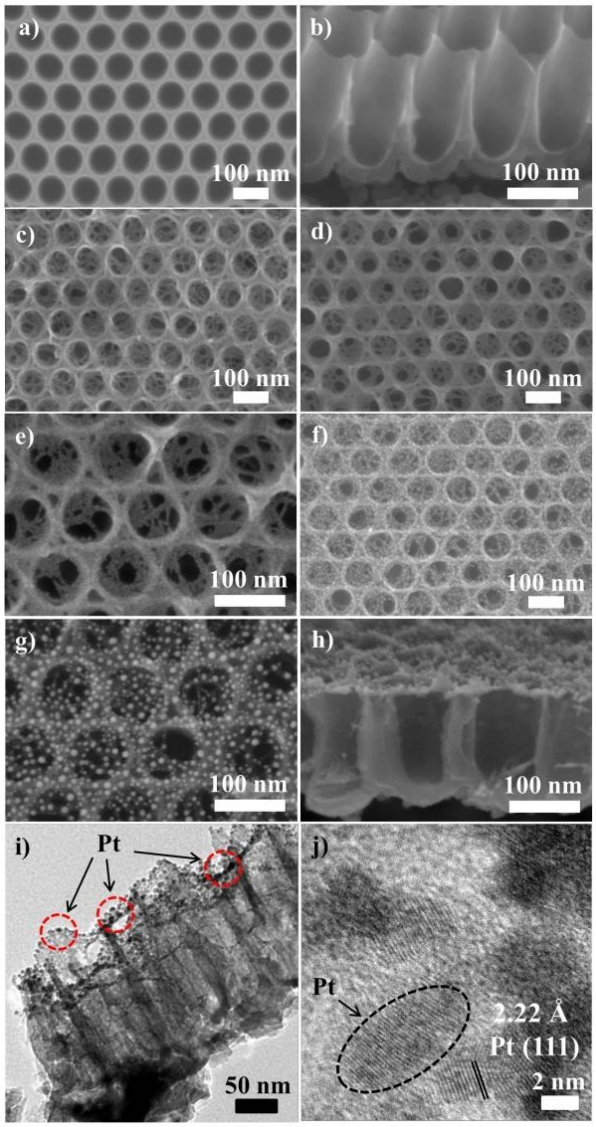

Fig. 1 SEM images of a), b) as-formed TiO_2 nanotubes; c) nanofibrils after 30 min-long NaOH-treatment; 1 nm-thick suspended Pt nanoparticles: d), e) before and f), g), h) after thermal dewetting in Ar; i) TEM image of suspended Pt nanoparticles and j) HRTEM image of Pt nanoparticles showing lattice constant of 2.22 Å corresponding to the (111) crystallographic plane.

Fig. 1(d)-(h) illustrate the top and cross-section views of the structures produced after depositing a 1 nm-thick Pt layer followed by thermal dewetting. Only very little difference can be observed when comparing the SEM pictures of the structures before and after Pt deposition (Fig. 1(c)-(e)), this suggesting that sputtering forms a rather conformal polycrystalline Pt layer which homogeneously coats the nanofibrils. On the other hand, the formation of Pt nanoparticles on the nanofibrils becomes apparent after a subsequent annealing in Ar atmosphere (450 °C – 30 min) (Fig. 1(f) and (g)), that is, the agglomeration into Pt nanoparticles is due to thermal dewetting. One may note that the Pt nanoparticles, though suspended at the top of the structures, do not block the access of the liquid phase towards the within of the tubes (this is clearly apparent in Fig. S2(f)). The Pt particles are a few nm in diameter (3-6 nm) and their size is related to the nominal thickness of the initially deposited Pt layer. In particular, the mean diameter of the Pt nanoparticles increases by increasing the thickness of the initial Pt layer (Fig. S3 and S4). When the nominal Pt thickness reaches a value of *ca*. 10-15 nm, the Pt nanoparticles tend to agglomerate forming a Pt layer that coats the nanotube walls and leaves nearly no Pt deposits on the fibrils (Fig. S3(f)-(g)). However, for thinner Pt films, the cross-sectional TEM image in Fig. 1(i) shows that the Pt nanoparticles are preferentially attached to the nanofibrils and suspended over the tube opening. The crystallinity of metallic Pt nanoparticles, strictly needed for efficient photocatalytic enhancement,[25] was confirm by TEM analysis, that is, the HR-TEM image in Fig. 1(j) shows a lattice constant of 2.22 Å corresponding well to the Pt (111) crystallographic plane.[26]

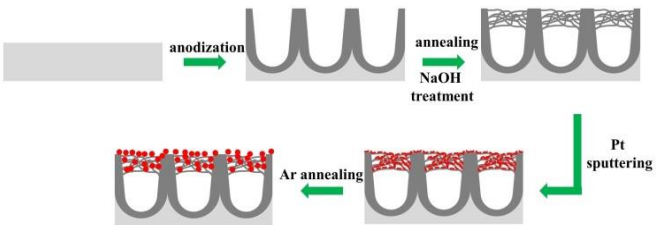

Scheme 1 Formation of suspended Pt nanoparticles over TiO_2 nanotubes: (i) anodization in hot H_3PO_4/HF electrolyte, (ii) first annealing in air and NaOH soaking, (iii) Pt sputtering and (iv) second annealing in Ar.

Fig. 2(a) shows XRD patterns that were collected for the structures at different stages of their fabrication. The as-formed tubes are amorphous while the first heat treatment in air induces the crystallization of TiO_2 into a mixed anatase-rutile phase. In our previous study, such phase composition of the tubes was found to be the most efficient for photocatalytic H_2 production.[5] The XRD patterns recorded for the Pt-decorated structures do not show any Pt peak when the sputtered film is thinner than 10 nm (such amounts of Pt might be undetectable by XRD). However, when the film is 15 nm-thick, Pt peaks (peaking at $2\Theta = 45.9°$ and 67.1°) clearly appear in the diffractograms. When 15 nm-thick Pt-decorated TiO_2 nanotubes undergo the second thermal treatment (in Ar, at 450 °C for 30 min), the intensity of Pt peaks clearly increases. This might be related to a higher degree of crystallinity of the Pt nanoparticles for the double-annealed materials. It has been also reported that Pt sputtered layers might show a relevant content of amorphous Pt oxides, *i.e.*, Pt(II) and Pt(IV) oxides.[27] Therefore, the second annealing in Ar atmosphere may induce the reduction of Pt oxides into Pt^0 along with the crystallite growth.

XPS characterization (Fig. 2(b)) was performed for the different structures, before and after Pt deposition, to examine the chemical state of the samples. The actual deposition of Pt is confirmed by the appearance of signals peaking at 72.06, 314.86 and 331.66 eV, these values corresponding to the binding energies of Pt 4f, 4d5 and 4d3, respectively. A signal peaking at 493.1 eV indicates the presence of Na that is ascribed to the sample treatment in NaOH.

Fig. 3(a) shows the amount of H_2 produced from water-ethanol solutions under UV illumination (laser, 325 nm, 60 mW cm^{-2}) for

structures decorated with different Pt amounts (nominal thickness in the 0-15 nm range).[4,15,18,19,28] While the bare structures (*i.e.*, Pt free) only lead to a production of 2.8 µL H_2 / 9 h, the Pt-decorated structures show, as expected, a much higher photocatalytic H_2 production rate (r_{H2}). The high activity of Pt@TiO_2 can be ascribed to the formation of Schottky junction at the interface between TiO_2 and the noble metal particle.[16,29] This induces efficient charge carrier separation as conduction band electrons are efficiently trapped by the Pt nanoparticles. By this, electrons are more readily available to reduce H_2O and generate H_2. The only a few nm thin Pt decorated fibrils provide very short carrier diffusion length to the Pt junction and this is perceived as a main beneficial effect. In particular, we observe that the r_{H2} drastically increased when a few nm-thick Pt films are deposited. A Pt thickness of 1 nm leads to the highest r_{H2} of 873 µL (*i.e.*, *ca.* 0.1 mL h^{-1}). In other words, only minimal amounts of Pt are needed in the suspended geometry to efficiently place the co-catalyst. For this photocatalyst, the amount of evolved H_2 linearly increases with irradiation time, *i.e.*, the r_{H2} is steady over time, confirming that neither release (fall-off) of Pt nanoparticles nor (photo-)corrosion of the structures takes place (Fig. S5). The structures decorated with a 1 nm-thick Pt layer already represent an optimum in view of photocatalytic H_2 production. When the Pt amounts are increased, a considerable drop of photocatalytic activity occurs. This may be due to *i)* a large increase of the mean size of Pt nanoparticles and *ii)* "shading effect", *i.e.*, larger amounts of deposited Pt optically shield the underneath structure so that the semiconductor is actually exposed to lower specific photon flux (Fig. S3).

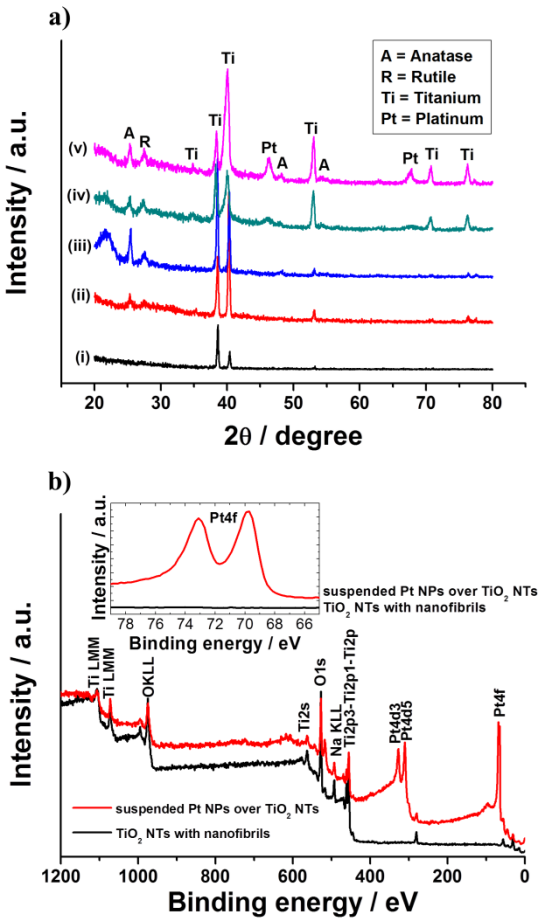

Fig. 2 a) XRD patterns of (i) as-formed TiO_2 nanotubes; (ii) annealed TiO_2 nanotubes; (iii) 1 nm-thick Pt suspended over TiO_2 nanotubes after thermal dewetting in Ar; 15 nm-thick Pt suspended over TiO_2 nanotubes (iv) before and (v) after thermal dewetting in Ar. b) XPS spectra of TiO_2 nanotubes with nanofibrils and suspended Pt nanoparticles (NPs) over TiO_2 nanotubes (NTs). The inset shows the enlarged area of the XPS spectra of Pt4f.

Fig. 3(b) shows a comparison of the photo-activity of different TiO_2 structures decorated with a 1 nm-thick Pt film. Both Pt@compact TiO_2 and Pt@TiO_2 nanotubes show a much lower r_{H2} compared to nanotubes decorated with suspended Pt nanoparticles (Fig. S6). The low efficiency of the compact film is clearly due to its low surface area. On the other hand, the low r_{H2} of Pt@TiO_2 nanotubes demonstrates that the nanofibrils represent a significant geometry improvement that drastically enhances the photocatalyst performance for the same Pt loading. Except for the short charge carrier diffusion length in the fibrils, another factor can be a direct diffusion access for the reactants (such as for a catalyst suspended into the reaction mixture). It is noteworthy that also the NaOH-soaking time affects the r_{H2}: a 30 min-long treatment leads to the most efficient photocatalyst while a loss of activity was observed when fibrils are too packed (60 min-long soaking), likely due to: *i)* hindered light penetration shadowing effects by formation of larger Pt nanoparticles (Fig. S7) and *ii)* a reduced exchange of the liquid phase through the fibrils into the tubes.

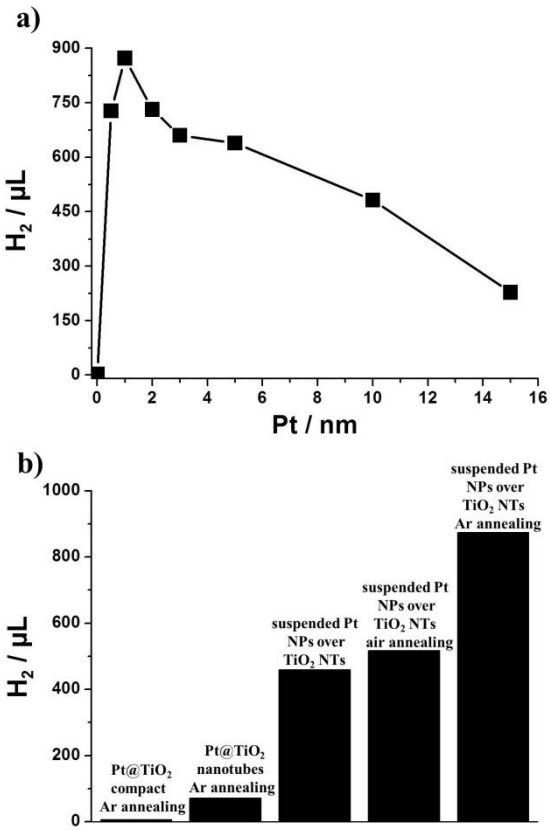

Fig. 3 Photocatalytic H_2 evolution measured for: a) TiO_2 nanotubes decorated with different nominal thicknesses of Pt; b) different types of TiO_2 structures all decorated with 1 nm-thick Pt layer. All experiments lasted 9 h and were carried out under UV light irradiation (HeCd laser, λ = 325 nm, power = 60 mW cm^{-2}).

In order to assess the light absorption properties of the different structures, UV-Vis diffuse reflectance spectra were collected and only a minor variation between the different morphologies was found although a significantly larger H_2 evolution was measured upon Pt nanoparticle decoration, as described above. Therefore, the large hydrogen production observed for the suspended Pt nanoparticles is likely not associated with optical features.

Another crucial point affecting the efficiency of the structures is the annealing treatment. As shown in Fig. 3(b), the tubes decorated with suspended Pt nanoparticles showed a doubling of r_{H2} after a second Ar-annealing. The reason for this is that as-formed fibrils are amorphous, and annealing is required to achieve conversion into crystalline oxide. Besides crystallization, the second Ar-annealing also causes the Pt dewetting and formation of Pt nanoparticles. The Ar-atmosphere during the second annealing is crucial. Experiments in where the second heat treatment was conducted in air (Fig. 3(b)) showed only a negligible increase of r_{H2} compared to single-annealed structures. Additional experiments were carried out using different treatment times of the second Ar-annealing or a different sputtering-annealing sequence (Fig. S8). In the first case, the highest r_{H2} was obtained with a 30 min-long Ar-treatment, this probably due to *i)* an optimized mean size and crystallinity of the Pt nanoparticles, and *ii)* optimized light absorption ability of the fibrils. If the second Ar-annealing is performed before Pt sputtering, a markedly low r_{H2} is obtained. Therefore, one might conclude that: *i)* Ar-annealing allows dewetting and induces crystallite growth and *ii)* Pt-dewetting partially exposes the fibrils, *i.e.*, it uncovers them and a larger photon flux can be absorbed.

Overall, in the present work we introduce the fabrication of a very efficient photocatalyst geometry that is based on Pt nanoparticles suspended over the top opening of highly ordered TiO_2 nanotubes. Their preparation is based on simple self-ordering processes. Only minimum amount of Pt is required to achieve strongly enhanced photocatalytic H_2 evolution efficiencies compared to conventional Pt decoration approaches.

The authors would like to acknowledge ERC, DFG and the DFG cluster of excellence EAM for financial support as well as H. Hildebrand for valuable technical help.

Notes and references

[a] Department of Materials Science and Engineering WW4-LKO, University of Erlangen-Nuremberg, Martensstrasse 7, D-91058 Erlangen, Germany.
[b] Department of Chemistry, King Abdulaziz University, Jeddah, Saudi Arabia
Email: schmuki@ww.uni-erlangen.de
Fax: +49-9131-852-7582;
Tel: +49-9131-852-7575

†Electronic Supplementary Information (ESI) available: [details of any supplementary information available should be included here]. See DOI: 10.1039/c000000x/

1 A. Fujishima and K. Honda, *Nature*, 1972, **238**, 37.
2 O. K. Varghese, D. Gong, M. Paulose, K. G. Ong, E. C. Dickey and C. A. Grimes, *Adv. Mater.*, 2003, **15**, 624.
3 I. Paramasivam, H. Jha, N. Liu and P. Schmuki, *Small*, 2012, **8**, 3073.
4 K. Lee, R. Hahn, M. Altomare, E. Selli and P. Schmuki, *Adv. Mater.*, 2013, **25**, 6133.
5 S. N. Basahel, K. Lee, R. Hahn, P. Schmuki, S. M. Bawaked and S. A. Al-Thabaiti, *Chem. Commun.*, 2014, **50**, 6123.
6 K. Lee, R. Hahn and P. Schmuki, *Electrochem. Commun.*, 2014, **43**, 105.
7 Z. Miao, D Xu, J. Ouyang, G. Guo, X. Zhao and Y. Tang, *Nano Lett.*, 2002, **2**, 717.
8 M. Assefpour-Dezfuly, C. Vlachos and E. H. Andrews, *J. Mater. Sci.*, 1984, **19**, 3626.
9 V. Zwilling, E. Darque-Ceretti, A. Boutry-Forveille, D. David, M. Y. Perrin and M. Aucouturier, *Surf. Interface Anal.*, 1999, **27**, 629.
10 K. Zhu, N. R. Neale, A. Miedaner and A. J. Frank, *Nano Lett.*, 2007, **7**, 69.
11 P. Roy, S. Berger and P. Schmuki, *Angew. Chem. Int. Ed.*, 2011, **50**, 2904.
12 J. M. Macak, M. Zlamal, J. Krysa and P. Schmuki, *Small*, 2007, **3**, 300.
13 S. K. Mohapatra, N. Kondamudi, S. Banerjee and M. Misra, *Langmuir*, 2008, **24**, 11276.
14 X. He, Z. Cai, H. Zhang and C. Liang, *J. Mater. Chem.*, 2011, **21**, 475.
15 A. Naldoni, M. D'Arienzo, M. Altomare, M. Marelli, R. Scotti, F. Morazzoni, E. Selli and V. D. Santo, *Appl. Catal., B*, 2013, **130-131**, 239.
16 A. L. Linsebigler, G. Lu and J. T. Yates, *Chem. Rev.*, 1995, **95**, 735.
17 J. Kiwi and M. Grätzel, *J. Phys. Chem.*, 1984, **88**, 1302.
18 U. G. Akpan and B. H. Hameed, *Appl. Catal., A*, 2010, **375**, 1.
19 N. J. Renault, P. Pichat, A. Foissy and R. Mercier, *J. Phys. Chem.*, 1986, **90**, 2733.
20 M. Ni, M. K. H. Leung, D. Y. C. Leung and K. Sumathy, *Renew Sust. Energ. Rev.*, 2007, **11**, 401.
21 J. E. Yoo, K. Lee, M. Altomare, E. Selli and P. Schmuki, *Angew. Chem. Int. Ed.*, 2013, **52**, 7514.
22 J. E. Yoo, K. Lee and P. Schmuki, *Electrochem. Commun.*, 2013, **34**, 351.
23 C. Wang, L. Yin, L. Zhang, N. Liu, N. Lun and Y. Qi, *ACS Appl. Mater. Interfaces*, 2010, **2**, 3373.
24 S.-H. Oh, R. R. Finones, C. Daraio, L.-H. Chen and S. Jin, *Biomaterials*, 2005, **26**, 4938.
25 G. L. Chiarello, M. V. Dozzi, M. Scavini, J.-D. Grunwaldt and E. Selli, *Appl. Catal., B*, 2014, **160-161**, 144.
26 D. Dang, S. Liao, F. Luo, S. Hou, H. Song and P. Huang, *J. Power Sources*, 2014, **260**, 27.
27 K. Kuribayashi and S. Kitamura, *Thin Solid Films*, 2001, **400**, 160.
28 G. L. Chiarello, D. Ferri and E. Selli, *J. Catal.*, 2011, **280**, 168.
29 O. Rosseler, M. V. Shankar, M. K.-L. Du, L. Schmidlin, N. Keller and V. Keller, *J. Catal.*, 2010, **269**, 179.

Graphical abstract